Structure-Property Correlation of Hypoeutectic Al-7.6Si Alloys with and without Al-5Ti-1B Grain Refiner

Prosanta Biswas[1], Sourabh Gupta[1,2], Manas Kumar Mondal[1]*, Rahul Bhandari[3] and Susanta Pramanik[1]

[1]Department of Metallurgical and Materials Engineering, National Institute of Technology, Durgapur 713 209, West Bengal, India

[2]Durgapur Steel Plant (Steel Authority of India Limited), Durgapur-713 203, West Bengal, India

[3]Luthfaa Polytechnic Institute, Durgapur-713 212, West Bengal, India

Hypoeutectic Al-7.6Si alloy has been developed with and without Al-5Ti-1B grain refiner through the gravity casting method. Effects of 2, 4, and 6 wt % master alloy (Al-5Ti-1B) addition on the microstructural morphology, mechanical properties (percentage elongation (%El) and ultimate tensile strength (UTS)), hardness and fracture behaviour of the Al-7.6Si alloy have been investigated. Unmodified hypoeutectic Al-7.6Si alloy consists of needle and rod-like eutectic Si ($(Si)_E$) particles with sharp corners inside the Al_α phase. In the grain refined Al-7.6Si alloy, TiB_2 is formed and these TiB_2 acts as a potential site for nucleation of Al_α grains. Therefore, the grain refined alloys have fine globular Al_α grains and fibrous $(Si)_E$ phase. The bulk hardness, UTS and elongation (%) are increased in the grain refined alloys. Further, fractography show that the cleavage fracture is reduced in the modified alloy and fine dimple formation is increased.

Keywords: Hardness, Fracture behaviour, Mechanical properties, Microstructure evolution, Phase analysis

Introduction

In aerospace and automotive industries, the aluminium based alloys[1–5] and composites[6–12] have an extensive application for their outstanding physical and mechanical properties. The Al-Si alloys are popular among Al- based alloys and composites. The hypoeutectic unmodified Al-Si alloy microstructure generally exhibits a coarse flake like $(Si)_E$ morphology.[13] Therefore, Al-Si alloy refinement and modification are needed to achieve improved mechanical properties. Previously, few researchers investigated the effect of varying ratios Ti and B modification on the Al-Si alloy.[14,15] However, minor amounts of Ti and B addition has a critical issue with the modification effects since Ti reacts with Si in the Al-Si alloy and forms $(Ti_{1-x}Si_x)Al_3$ compounds. Therefore, Al_3Ti and TiB_2 intermetallic formation are decreased; thus, the nucleation site for Si phase and primary Al (Al_α) grains reduces.[14,16] In this research, hypoeutectic Al-7.6 Si alloy has been successfully synthesized through simple gravity die casting technique with (2 wt.%, 4 wt.% and 6wt.%) and without Al-Ti-B grain refiner. The objective of this study is to explore the influence of higher concentration Ti and B addition on the elongation, UTS and hardness of the hypoeutectic Al-7.6Si alloy. Finally, a correlation is established between the microstructural morphology and mechanical properties to understand the various aspects of properties modulation.

Experimental Details

The hypoeutectic Al-7.6Si alloy was synthesized through the gravity die casting method. Firstly, small pieces of Al (99.7% commercial purity) were melted using an electrical resistance furnace at 760°C in a SiC-clay graphite-based crucible. After melting of commercially pure Al, small pieces of pure silicon (99.16%) was added into the melt and held for complete Si dissolution (45 minutes). Then, the Al-Ti-B master alloy was added into the molten metal and again waited for 20 minutes. In this period, the molten metal was stirred manually using a graphite rod in an interval of 5 minutes. Then the molten metal was degassed with hexachloroethane (0.1 wt.%). The slag was removed from the top portion of the melt and the molten alloy was quickly poured into a preheated cast iron (CI) mould, designed as per BS1490 standard.[17]

After solidification, optical metallography and hardness test samples (10 mm × 10 mm × 5 mm) were cut out from the as-cast billets. The metallography samples were polished through the standard procedure

—————
*Author for Correspondence
E-mail: manas.nitdgp@gmail.com

and etched with a solution of 1% HF, 1.5% HCl, 2.5% HNO₃ and 90% distilled water called Keller's reagent. The optical microscopy was carried out by Leica optical microscope. Hardness test was done on the Vicker's hardness testing machine. PAN alytical X'Pert PRO machine with Cu-K$_\alpha$ radiation was used for XRD analysis. Further, round shape tensile test samples (as per ASTM standard) were machined out from the cast billet. The tensile test was performed by Tinius Olsen Universal Testing Machine at room temperature. Fracture surfaces were investigated using a FESEM (Carl Zeiss, Sigma, UK) to understand the mode of fracture. The volume percentage (stereological equal to area percentage) of different phases and α-Al grain size were measured using the ImageJ image analysis software considering 10 image frames.

Results and Discussion

Microstructural Evaluation

The optical microstructures of the Al-7.6Si alloy with and without refiner are shown in Fig. 1(a)–(d). The unmodified hypoeutectic Al-7.6Si alloy (Fig. 1(a)) displays a grey colour dendritic plate-like and needle-like phase inside the Al$_\alpha$ phase. This grey colour phase is identified as the eutectic Si ((Si)$_E$) phase by the EDS spot analysis (shown in Fig. 2 (a)). The (Si)$_E$ phase is evenly distributed within the Al phase which appears like a matrix. The (Si)$_E$ particles have sharp corners; those are the preferable sites for stress concentration and failure initiation during loading.

Addition of 2 wt.%, 4 wt.% and 6wt.% grain refiner (Al-5Ti-1B) effectively modify and refine both the Al$_\alpha$ and (Si)$_E$ phase (Fig. 1(b)–1(d)). The alloy with 2.0 wt.% grain refiner has some globular α-Al grains with dendritic morphology and a fibrous (Si)$_E$ phase with large spacing (Fig. 1(b)). Further, the Al-7.6Si-4 wt.% Al-5Ti-1B alloy has more amount of globular Al$_\alpha$ grains and a fine fibrous (Si)$_E$ morphology with least spacing compared to the 2.0 wt.% grain refined alloy (Fig. 1(c)). The Al$_\alpha$ grains average diameter decreases and roundness (degree of sphericity (DOS)) increases, when the concentration of the grain refiner is increased from 2.0 wt.% to 4.0 wt.% (Table 1). But, the alloy with 6.0 wt.% grain refiner has more dendritic Al$_\alpha$ grains with less roundness and the spacing of fibrous (Si)$_E$ is more as compared to the alloy with 4 wt.% grain refiner (Fig. 1(d)). The averaged Al$_\alpha$ grain size is also comparatively large and roundness is less (Table 1). This may have resulted from over modification of the alloy. The averaged Al$_\alpha$ grain size and DOS were estimated by ImageJ analysis software and estimated using to Eqs (1) and (2).[18-19]

$$Grain\ Diameter\ (GD) = 2\sqrt{A_g/\pi} \qquad \cdots (1)$$

$$Roundness(R) = \left(4\pi A_g/P_g^2\right) \qquad \cdots (2)$$

Where A_g is the area and Pg is the perimeter of the Al$_\alpha$ grains.
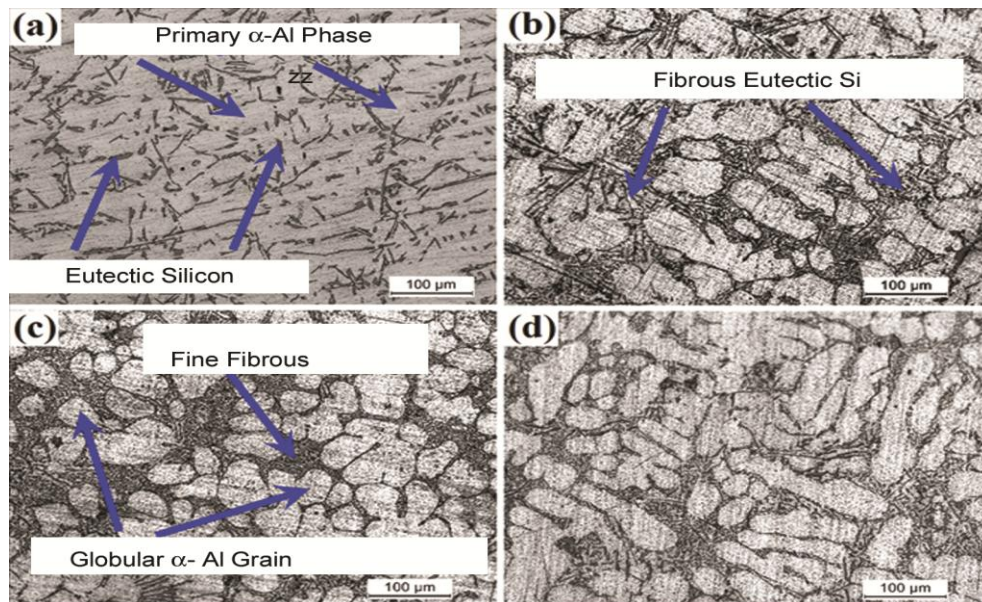

Fig. 1 — Optical microstructure of (a) Al-7.6 Si alloy (b) Al-7.6 Si alloy with 2 wt. % Al-5Ti-1B (c) Al-7.6 Si alloy with 4 wt. % Al-5Ti-1B and (d) Al-7.6 Si alloy with 6 wt. % Al-5Ti-1B
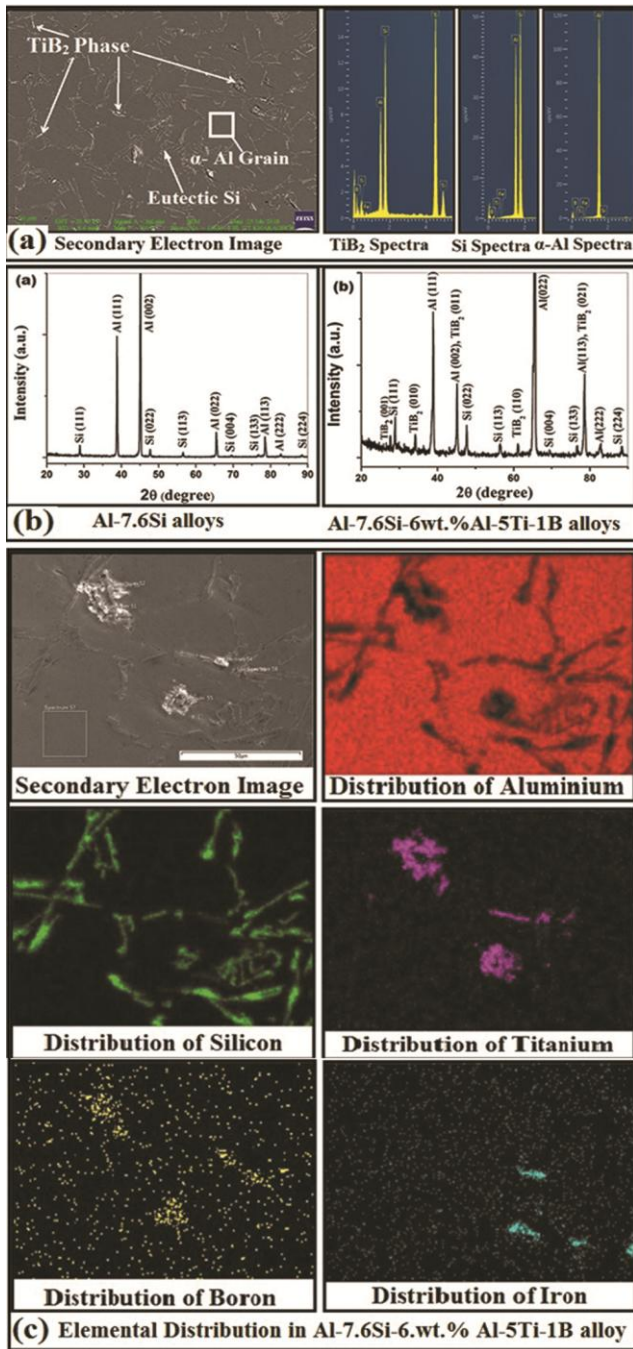
Fig. 2 — Phase identification by : (a) SEM based EDX spot analysis (b) XRD analysis and (c) SEM with elemental mapping

Furthermore, the X-ray diffractogram of the Al-7.6Si alloy with and without grain refiner (Al-5Ti-1B) displays the peaks of Al and Si, whereas the 6 wt.% grain refineradded alloy has the peaks of titanium diboride (TiB_2) other than the Al_α and Si peaks (Fig. 2(b)). Further, SEM-based EDS spot analysis confirms the presence of TiB_2 (Fig. 2(a)) and

elemental mapping (Fig. 2(c)). The TiB_2 posses HCP structure with a lattice parameter $a_{TiB2} = b_{TiB2} = 3.034$ Å, $c_{TiB2} = 3.226$ Å[20] and the crystal structure of aluminium is FCC with a lattice parameter $a_{Al} = 4.0497$ Å.[21] The FCC aluminium matrix has (111) closed packed plane matching with (0001) closed packed plane of the HCP TiB_2. The closed packed direction on (0001) plane is 2110 and the interatomic distance is a_{TiB2}. Further, interatomic distance in closed packed [110] direction on (111) plane is $a_{Al}/\sqrt{2}$ and the misfit parameter is 0.056. Therefore, the TiB_2 acts as potential nucleation sites of Al_α grains during solidification. The modification and refinement of both the phases occur due to the formation of the TiB_2 in the grain refined alloy.

Hardness

The bulk hardness of the alloys and composites generally depends on the microstructural morphology of the alloys.[17] The bulk hardness of the developed alloys with increased wt. % of grain refiner is shown in Table 1. The bulk hardness of unmodified alloy is approximately 46 HV0.1, but the modified alloys have a bulk hardness around 64HV0.1 to 75HV0.1. This increase in hardness is caused by the microstructural morphology change, such as globular Al_α grains and fibrous $(Si)_E$ phase formation in the modified alloy. The Al-7.6Si-4.wt% Al-5Ti-1B alloy has a higher hardness value compare to other modified alloy because it has more globular fine Al_α grains and fibrous $(Si)_E$ phase with low spacing.

Mechanical properties

The mechanical properties (elongation and UTS) of the synthesized alloy with increased wt.% of grain refiner is shown in Table 1. The un-modified Al-7.6Si alloy has a UTS and percentage elongation of 108 MPa and 6.60%, respectively. The grain refinement of synthesized alloy by the addition of 2.0 wt.% grain refiner resulted in 33.3% and 47.5% improvement of UTS and percentage elongation values, respectively. The Al-7.6Si-4 wt.% Al-5Ti-1B refined alloy has comparatively more improved UTS (58.3%) and percentage elongation (101.5%) with reference to unmodified alloy. But, further increase in the grain refiner concentration to 6 wt.% the elongation and UTS values slightly decreased compared to Al-7.6Si-4 wt.% Al-5Ti-1B, but much higher than the unrefined alloy. This improvement of the UTS and ductility attribute to microstructural refinements such as fine globular α-Al grains and fibrous $(Si)_E$ phase

Table 1 — Microstructural features, hardness and mechanical properties of Al-5Ti-1B added Al-7.6Si alloys

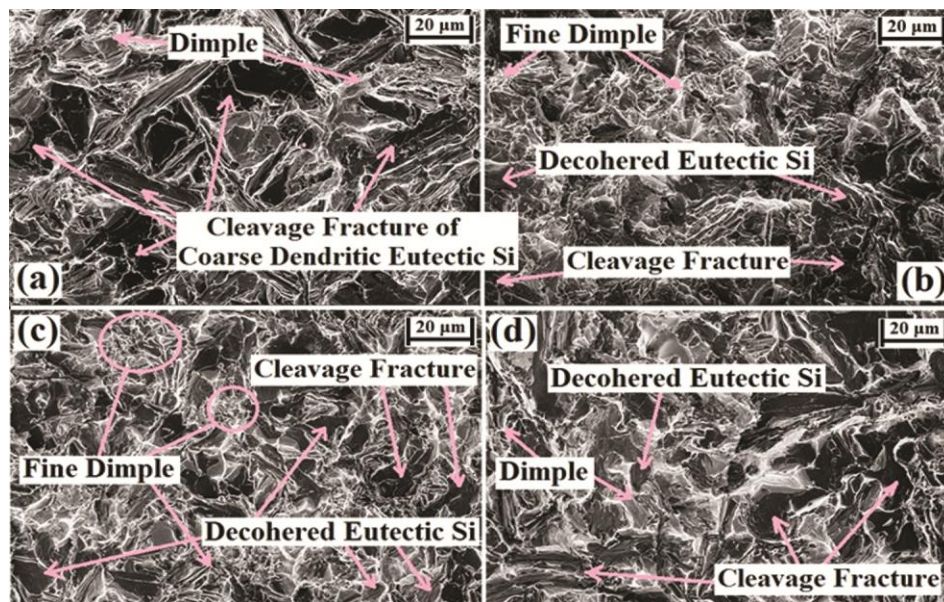| Alloy	α- Al grain mean dia. (μm)	α- Al grain Aspect Ratio	α- Al phase vol. (%)	Binary eutectic (Al-Si) phase vol. (%)	Hardness (HV0.1)	Ultimate Tensile Strength (MPa)	Elongation (%)
Al-7.6 Si-0.0 wt. % Al-5Ti-1B	—	—	86.63	13.37	46±1.5	106±5.20	6.6±0.50
Al-7.6 Si-2.0 wt. % Al-5Ti-1B	57.6	0.655	72.5	27.75	65±1	143±6.70	9.75±0.35
Al-7.6 Si-4.0 wt. % Al-5Ti-1B	42.4	0.692	65.76	34.24	74±1	171±2.25	13.35±0.42
Al-7.6 Si-6.0 wt. % Al-5Ti-1B	51.5	0.677	74.68	25.32	71±1	166±3.5	10.6±0.40

Fig. 3 — SEMSecondary electron images of the fractured surfaces: (a) Al-7.6Si alloy (b) Al-7.6Si-2 wt.% Al-5Ti-1B alloy (c) Al-7.6Si-4 wt.% Al-5Ti-1B alloy and (d) Al-7.6Si-6 wt.% Al-5Ti-1B alloy

with low spacing. Bhandari *et al.*[22] also found that the consisting phases morphology has a significant influence on aluminium based alloys'mechanical response.

Fractographic studies

The synthesized alloys fracture surfaces are shown in Fig. 3. It is well established that the various structural defects (micro-porosity and microcrack) and sharp corners of particles act as proper sites for failure to begin. The crack propagation through the $(Si)_E$ particles by means of cleavage fracture are shown in Fig. 3 (a) & (d). However, a combined mode of fracture (brittle and ductile) with dimple formation has been found in the fracture surface of the developed alloys. The dimples generally occurs for the existence of the secondary phase particles, which results in the interfacial decohesion.[23] The fractography of the unmodified alloy has mainly

cleavage facets of coarser and dendritic $(Si)_E$ particles (Fig. 3(a)). Whereas, the grain refined alloys have a very less number of cleavage fracture of $(Si)_E$ as the plate-like and needle-like $(Si)_E$ transformed into fibrous morphology. The decohered particles are observed in the grain refined alloy and the dimple formation has also increased (Fig. 3(c)–(d)). A great agreement has been found between the fracture surface fractography and UTS, elongation and microstructural morphology of the synthesized alloys.

Conclusions

Microstructure, mechanical properties, hardness and fracture behavior of the hypoeutectic Al-7.6Si alloy has been investigated with respect to grain refiners' (Al-5Ti-1B) concentration and the following conclusions are drawn:

The unmodified hypoeutectic alloy consists of a needle and rod-like $(Si)_E$ particles with sharp corners

inside the Al_α phase and the Al_α phase is present as a matrix phase. The grain refined alloys have globular Al_α grains and a fibrous $(Si)_E$ phase. The elongation values, UTS and bulk hardness of the developed alloy have increased in the grain refined alloy.

Addition of 4 wt.% of grain refiner (Al-5Ti-1B) to the Al-7.6Si alloy gave the smallest grain size and highest roundness of Al_α grains compare to the 2 wt.% and 6 wt.% of grain refiner addition. As a result, the Al-7.6Si alloy with 4 wt.% grain refiner has the highest strength (171 ± 2), ductility (13.3 ± 0.4) and hardness (73.8 ± 0.5).The cleavage fracture and brittle fracture are reduced and fine dimple formation is increased in the modified alloy.

Acknowledgements

References

1   Biswas P, Prasadu K D&Mondal M K, Effect of Bi addition on microstructure and mechanical properties of hypereutectic Al-17.6Si alloy, *Mat Res Exp*, **6** (2019) 1165b9.

2   Biswas P, Patra S, Roy H, Tiwary C S, Paliwal M & Mondal M K, Effect of Mn addition on the mechanical properties of Al$_{12.6}$Si alloy: Role of $Al_{15}(MnFe)_3Si_2$ intermetallic and microstructure modification, *Met Mater Int*, (2019), DOI: 10.1007/s12540-019-00535-5.

3   Biswas P, Bhandari R, Mondal M K & Mandal D, Effect of microstructural morphology on microscale deformation behavior of Al-4.5Cu-2Mg alloy, *Arch Metall Mater*, **63** (2018) 1575–1586.

4   Biswas P, Patra S & Mondal M K, Effects of Mn addition on microstructure and hardness of Al-12.6Si Alloy, *IOP Conf Series: Mater Sci Eng*, **338** (2018) 012043.

5   Basak S, Biswas P, Patra S, Roy H & Mondal M K, Effect of TiB$_2$ and Al$_3$Ti on Microstructure, Mechanical Properties and Fracture Behaviour of Near Eutectic Al-12.6Si Alloy, *Int J Miner Metall Mater*, https://doi.org/10.1007/s12613-020-2070-8

6   Kakhki Y S, Nategh S & Mirdamadi S, Prediction of porous Al/SiC nanocomposite creep behaviour via the mechanical alloying process, *Indian J Eng Mater Sci*, **24** (2017) 27–34.

7   Kumar T S, Subramanian R, Shalini S & Angelo P C, Age hardening behaviour of Al-Si-Mg alloy matrix/Zircon and alumina hybrid composite, *J Sci Ind Res*, **75** (2016) 89–94.

8   Jailani H S, Rajadurai A, Mohan B & Sornakumar T, Evaluation of drilled hole quality of Al-Si alloy/fly ash composites produced by powder metallurgical technique, *Indian J Eng Mater Sci*, **22** (2015) 414–420.

9   Kumar T S, Subramanian R, Shalini S, Anburaj J & Angelo P C, Synthesis, microstructure and mechanical properties of Al-Si-Mg alloy hybrid (Zircon+Alumina) composite, *Indian J Eng Mater Sci*, **23** (2016) 20–26.

10   Biswas P, Mondal M K & Mandal D, Effect of Mg_2Si concentration on the dry sliding wear behavior of Al–Mg_2Si composite, *ASME J Tribol*, **141** (2019) 081601.

11   Bhandari R, Mallik M & Mondal M K, Microstructure evolution and mechanical properties of in situ hypereutectic Al-Mg_2Si composites", *AIP Conf Proc*,**2162** (2019) 020145.

12   Biswas P, Mandal D & Mondal M K, Micromechanical response of Al-Mg_2Si composites using approximated representative volume elements (RVEs) model, *Mater Res Express*, **6** (2019), 1165c6.

13   Eiken J, Apel M, Liang S M & Fetzer R S, Impact of P and Sr on solidification sequence and morphology of hypoeutectic Al–Si alloys: Combined thermodynamic computation and phase-field simulation, *Acta Mater*, **98** (2015) 152–163.

14   Birol Y, Effect of silicon content in grain refining hypoeutectic Al–Si foundry alloys with boron and titanium additions, *Mater Sci Technol*, **28** (2012) 385–389.

15   Auradi V & Kori S A, Effect of processing temperature on the microstructure of Al-7Ti master alloy and on refinement of α-Al dendrites in Al-7Si alloys, *Adv Mater Lett*, **6** (2015) 252–259.

16   Biswas P, Patra Sand Mondal M K, Structure-property correlation of eutectic Al-12.4 Si alloys with and without Zirconium (Zr) addition, *Int J Cast Met Res*,DOI: 10.1080/13640461.2020.1769319

17   Biswas P, Mondal M K, Roy H & Mandal D, Microstructural evolution and hardness property of in situ Al–Mg_2Si composites using one-step gravity casting method, *Can Metall Q*, **56** (2017) 340–348.

18   Zhang L J, Fan J T, Liu D J, Zhang M D, Yu P F, Jing Q, Ma M Z, Liaw P K, Lia G & Liu R P, The microstructural evolution and hardness of the equiatomic CoCrCuFeNi high-entropy alloy in the semi-solid state, *J Alloys and Compd*, **745** (2018) 75–83.

19   Arrabal R, Mingo B, Pardo A, Mohedano M, Matykina E, & Rodríguez I, Pitting corrosion of rheocast A356 aluminium alloy in 3.5 wt.% NaCl solution, *Corros Sci*, **73** (2013) 342–355.

20   Yan H Y, Qun W, Chang S, M & Ping G, U, A first-principle calculation of structural, mechanical and electronic properties of titanium borides, *Trans Nonferrous Met Soc China*, **21** (2011) 1627–1633.

21   Stock S R & Cullity B D, *Elements of X-ray Diffraction* (Addison-wesley publishing company, New York, USA) 1978, 506.

22   Bhandari R, Biswas P, Mondal M K & Mandal D, Finite element analysis of stress−strain localization and distribution in Al−4.5Cu−2Mg alloy, *Trans Nonferrous Met Soc China* **28** (2018) 1200−1215.

23   Biswas P, Biswas A, Bhandari R & Mondal M K, Microstructure, mechanical properties and fracture behavior of in-situ Al-5Mg-Al$_4$Sr composites, *Mater Today Comm*, **15** (2018) 190–198.